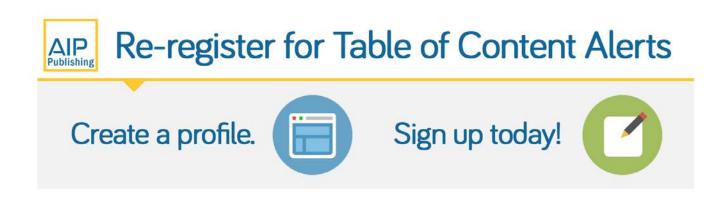# Thermal analysis of silver nanoparticles for flexible printed antenna fabrication

Krishnamraju Ankireddy, Mina Iskander, Swathi Vunnam, Dimitris E. Anagnostou, Jon Kellar, and William Cross

CrossMark
click for updates

Thermal analysis of silver nanoparticles for flexible printed antenna fabrication

Krishnamraju Ankireddy,[1] Mina Iskander,[2] Swathi Vunnam,[2] Dimitris E. Anagnostou,[3] Jon Kellar,[1] and William Cross[1]

[1]*Department of Materials and Metallurgical Engineering, South Dakota School of Mines and Technology, 501 East Saint Joseph St., Rapid City, South Dakota 57701, USA*
[2]*Program of Nanoscience and Nanoengineering, South Dakota School of Mines and Technology, 501 East Saint Joseph St., Rapid City, South Dakota 57701, USA*
[3]*Department of Electrical and Computer Engineering, South Dakota School of Mines and Technology, 501 East Saint Joseph St., Rapid City, South Dakota 57701, USA*

In this study, the temperature assisted decomposition/desorption behavior of short-chain single and mixed carboxylic acid encapsulants from the core of silver nanoparticles was investigated using thermogravimetric analysis and differential scanning calorimetry, and these particles were used to fabricate a flexible printed antenna. The decomposition temperatures of the single encapsulant particles increased with increasing chain length of encapsulants, whereas the decomposition temperatures for mixed encapsulant particles are close to the average of the corresponding decomposition temperatures of single encapsulant nanoparticles. These experimentally identified decomposition temperatures were utilized for sintering the printed antenna on a flexible substrate. The printed antenna showed a significantly low return loss of 22 dB. The antenna performance and radiation pattern are similar to a reference prototype antenna made of copper. © 2013 AIP Publishing LLC. [http://dx.doi.org/10.1063/1.4822159]

I. INTRODUCTION

Development of printed electronics/organic electronics strongly relies on the availability of printing material. Especially, nanoparticle-based materials are the most promising candidates for printing micro-electrodes,[1,2] flexible antennas,[3] organic thin film transistors,[4] radio frequency identification tags,[5] batteries,[6] and bio-circuits.[7,8] Most of these nanomaterials are sterically stabilized with surfactant/encapsulant molecules at the nanoparticle surface to prevent coalescence. These surfactants have to be removed from the core of the nanoparticles to make the printed patterns conductive. Thermal sintering is one route for heating the printed patterns so that the surfactants desorb from or decompose at the surface of the particles and initiate sintering process. The surfactant and its chain length play an important role in sintering behavior of the particle.

Thermal desorption of various encapsulants from the core of nanoparticles has been reported to some extent.[9–12] Thermogravimetric analysis (TGA) of decanoate protected silver nanoparticles showed two desorption maximum peaks at 181 and 263 °C which were ascribed to weakly and strongly chemisorbed decanoate onto the nanoparticles.[13] Desorption behavior has been studied with temperature programmed desorption spectroscopy (TPD) experiments for various chain length alkanethiol monolayers on Au (111) surface. These experiments showed two desorption peaks for octadecanethiol self assembled monolayer (SAM) on Au (111). These two peaks were thought to occur because of dimerization of octadecanethiol.[14,15] Relationships between structure and solubility of thiol-protected silver nanoparticles and assemblies were reported by Bauer *et al*.[9]

The TGA studies on these nanoparticles showed that the mass loss occurred after 250 °C. From differential scanning calorimetry (DSC) experiments, it was found that silver nanoparticles with a low energy of ligand disordering showed an increased solubility in organic solvents. TGA analysis of gold nanoparticles encapsulated with C4 chain length alkanethiol exhibited the lowest onset-decomposition temperature compared to C8 and C12 chain alkanethiol encapsulated particles because of the low boiling point of C4 alkanethiol.[10] Coutts *et al*.[12] reported that the sintering environment also influence the decomposition of encapsulant from the nanoparticles. TGA experiments conducted under a vacuum environment showed a greatly reduced chain length effect on the sintering process. Sintering was much faster in air than under an argon atmosphere. Much of the research has been done on gold and silver nanoparticles encapsulated with alkanethiols but not on carboxylic acids encapsulated silver nanoparticles. One simulation study showed that the binding energy for amine functional group on the low index silver surfaces is higher than the binding energies of carboxylic acids on same silver surfaces.[16] Low binding energy may be desired to desorb the encapsulant more easily from the core of the nanoparticles and initiate the sintering process. In particular, understanding the sintering temperatures of the particles before they are used for printing various patterns is necessary for selecting the substrate and printing system.

Metallic nanoparticles in printed electronics technology, especially for flexible antennas, have potential applications in new telecommunication systems.[17,18] The performance of printed antennas mainly relies on the printed materials, the antenna shape, and the conductivity

of the ink after sintering.[19,20] Most flexible antennas in the literature have been fabricated either using milling or etching technology and only few of them were printed using nanoinks.[3,21] The thermal analysis of silver nanoparticles conducted in this work may be useful to select a substrate which will not deform at the required sintering temperatures.

In this study, TGA and DSC experiments were conducted on the silver nanoparticles to understand the temperature assisted decomposition/desorption behavior of surfactants. A substrate was selected using the sintering temperatures obtained from the thermal analysis study and a direct-write printed, coplanar, and flexible folded-slot dipole antenna was made. The performance of the printed antenna was evaluated and compared to a similar antenna made of copper.

II. EXPERIMENTAL

Synthesis of silver nanoparticles was carried out using modified method of Lee *et al.*[22] which we recently reported.[1] Silver nitrate of 12.74 g was dissolved in n-butylamine of 20 ml and stirred at 400 rpm. Decanoic acid (99%, Alfa Aesar), octanoic acid (99.9%, Sigma Aldrich), and hexanoic acid (99.9%, Sigma Aldrich) were used without further purification. Single (C6, C8, and C10) and mixed chain (C6/C8, C6/C10, and C8/C10) carboxylic acids were used as surfactants to cap the nanoparticles. In this work, C6 means particles capped with hexanoic acid (6 carbon chain) and C6/C8 means the particle capped with mix of both hexanoic acid and octanoic acid. Same strategy is followed for other particles too. Single or mixed carboxylic acids with total of 0.0348 mol was added to 22.5 ml of toluene and transferred to the silver solution. Sodium borohydride of 2.84 g was added to the solution and refluxed for an hour. After refluxing, particles were cleaned with acetone and methanol, and filtered using a polytetrafluoroethylene (PTFE) membrane with a pore size of 220 nm.

Thermal analysis of silver nanoparticles was carried out using a DSC Q100 and an SDT Q 600 both from TA instruments and was performed under nitrogen atmosphere. In both sets of experiments, the temperature of the dried nanoparticles was ramped from 40 to 280 °C with the ramp rate of 10 °C/min. The printing of the antenna pattern was carried out under ambient conditions using an aerosol jet system from Optomec®. The ink used for the printing contains C10 particles with the concentration of 64 wt. % in toluene. Kapton® was mounted on the sample stage, and a 250 μm deposition tip was mounted to print head. Printing parameters were adjusted to sheath gas flow of 30 ccm, atomizer voltage of 50 V, and atomizer flow of 25–35 ccm. The sintering of the printed antenna was carried out using a Eurotherm furnace from Carbolite with the ramp rate of 10 °C/min. A Zeiss Supra 25 FE scanning electron microscope (SEM) at 6 kV accelerating voltage was used to analyze the microstructure of the printed pattern. The printed antenna high-frequency measurements were conducted using an Agilent™ E8361C PNA Network Analyzer (10 MHz to 67 GHz).

III. RESULTS AND DISCUSSION

A. Thermal analysis of the silver nanoparticles

The silver nanoparticles were having a narrow size distribution with the average diameter of 4.1 to 4.7 nm. Their structural properties, ink preparation, and ink properties were reported except thermal analysis of these particles and their application towards a device fabrication.[1] Figures 1(a) and 1(b) show the TGA curves for C6, C8, C10 as well as mixed encapsulants nanoparticles. From TGA, the weight loss from C6, C8, and C10 particles are 7%, 10%, and 15%, respectively. The weight loss from the nanoparticles increased with the increased chain length of the encapsulant. This is mainly because of the increased molecular weight with the increased chain length of the encapsulant. From Figure 1(b), the weight loss from C6/C10 encapsulated nanoparticles is 12% which is in between the weight loss of C6 and C10 particles. The weight loss from C8/C10 encapsulated particles is 13% as expected. But in case of C6/C8 particles, the weight loss is 11% which is greater than the weight loss from individual C6 or C8 nanoparticles. This implies that the C6/C8 encapsulated particles exhibit greater coverage of encapsulant molecules per unit area compared to corresponding C6 and C8 nanoparticles. The weight loss obtained from TGA analysis was used to estimate the area covered by the carboxylic acids on a nanoparticle. For example, area covered by the C6 capping molecules was approximately 63% of total surface area of a C6 nanoparticle. In case of C10 nanoparticles, approximately 90% of nanoparticle's area was covered by the C10 capping molecules. The coverage of both C6 and C10 capping molecules on a C6/C10 nanoparticle was 79% which is close to the average of the area coved by single C6 and C10 capping agents on the nanoparticles. This implies that the C6/C8 encapsulated particles exhibit greater coverage of encapsulant molecules per unit area compared to corresponding C6 and C8 nanoparticles. These weight loss values represent the mass fraction of the encapsulant in the nanoparticle. In order to verify the mass loss from the TGA experiments was only from the encapsulant of the nanoparticles, mass heating test and theoretical calculations were carried out on C6/C10 particles. Mass heating tests were conducted by taking a known weight of particles and heating at 230 °C for 17 h. The encapsulants were evaporated at that temperature, and weight of the silver content was measured. The mass fraction of the encapsulant to the particle was 16%. Theoretical calculations were carried out by creating a Connolly surface[23] of COO head group and considering this as a sphere. From theoretical calculations, mass fraction of the encapsulant to the nanoparticle was 12%. The mass fractions obtained from all three approaches closely match each other.

The peaks from the first derivative curve of TGA (Figure 1(c)) were originated due to the maximum decomposition/desorption of encapsulant occurred at those particular temperatures. These first derivative curves possess broad peaks which mean there is an overlap of multiple peaks.[24] Therefore, second derivative of TGA curves were obtained to separate individual peaks (Figure 1(c)). These individual
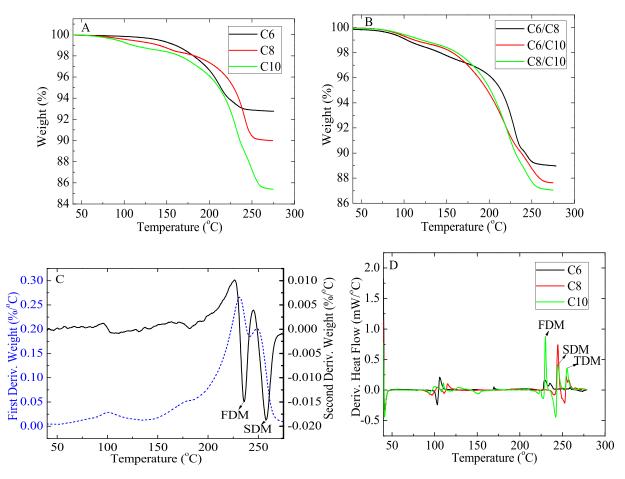
FIG. 1. (a) TGA curves for C6, C8, and C10 particles. (b) TGA curves for C6/C8, C6/C10, and C8/C10 particles. (c) First derivative and second derivative TGA curves for C10 particles. (d) First derivative DSC curves of C6, C8, and C10 particles.

peaks were compared with the first derivative curves obtained from the DSC experiments (Figure 1(d)) and tabulated in Table I. From Table I, the maximum decomposition temperatures obtained from the TGA are in good agreement with the DSC results. The C6 particles exhibited the first maximum decomposition (FMD) and the second maximum decomposition (SMD) temperatures at 219 and 236 °C, respectively. In case of C8 particles, there was a single maximum decomposition temperature at 246 °C from TGA. From DSC, the SMD for the C8 particles is at 254 °C. For mixed C6/C8 particles, FDM and SDM temperatures are

235 and 249 °C, respectively, which are close to the average of decomposition temperatures of C6 and C8 individual particles. This phenomenon is also observed in other single and mixed encapsulant particles (Table I). The TGA and DSC data from all the particles reveal that the decomposition temperatures of the single encapsulant particles increased with increasing encapsulant's chain length, whereas the decomposition temperatures for mixed encapsulant particles are close to the average of the corresponding decomposition temperatures of single encapsulant nanoparticles. The first derivative curves of TGA for all the nanoparticles retain a small peak around 100 °C which is also observed in the DSC curves (Figure 1). These peaks are believed to be caused by moisture and residual solvent loss from the nanoparticles. Although mass loss from all the nanoparticles was observed starting around 140 °C, the maximum mass loss occurred at higher temperatures. The amount of oxygen in the sintering process may influence the sintering temperature of gold and silver nanoparticles.[12] It might have been possible to increase the sintering rate of the nanoparticles using air instead of nitrogen atmosphere for TGA experiments. The origin of multiple desorption maxima from TGA data and the multiple exothermic peaks from the DSC data could be assigned to weakly and strongly chemisorbed encapsulants on the silver surface or dimerization of carboxylic acids and subsequent desorption of the dimer from the silver surface.[13–15]
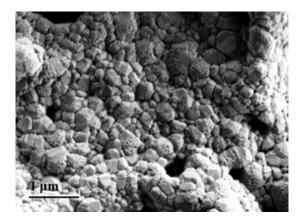
TABLE I. The maximum decomposition temperatures of the nanoparticles from TGA and DSC experiments.

Ag NPs	TGA		DSC		
	T_{FDM} (°C)[a]	T_{SDM} (°C)[b]	T_{FDM} (°C)	T_{SDM} (°C)	T_{TDM} (°C)[c]
C6	219	236	229	236	…
C8	246	…	244	254	…
C10	236	258	230	245	255
C6/C8	235	249	236	246	250
C6/C10	227	260	226	243	251
C8/C10	230	253	226	246	259

[a]T_{FDM} is the first decomposition maximum temperature.
[b]T_{SDM} is the second decomposition maximum temperature.
[c]T_{TDM} is the third decomposition maximum temperature.

FIG. 2. SEM image of sintered pattern at 240 °C for an hour.

B. Antenna printing and characterization

After identifying the decomposition temperatures of C10 encapsulants, nanoparticulate inks with C10 nanoparticles were chosen for printing. Kapton® was chosen as a substrate to support the printed flexible antenna, because it does not degrade around 240 °C. Kapton® was cleaned only with acetone before printing and no other surface treatments were performed. Substrate cleanliness and surface treatments play an important role in the dimensions and quality of the printed patterns.[25] The printed antenna was sintered for 1 h at 240 °C which was determined from Table I. Figure 2 shows a SEM image of the sintered pattern. The microstructure of the pattern shows that coalescence of the particles took place at this temperature and formed large grains. The conductivity of the printed antenna metallic surface after sintering was 2.96×10^7 S/m which is 47% of bulk silver conductivity (6.3×10^7 S/m). The electrical resistance of the printed pattern was measured with a Keithley 2400 source meter using the four-point probe method.

The coplanar folded slot antenna (CFSA) was printed on Kapton® substrate and sintered. A photo of the fabricated prototype is shown in Figure 3. The antenna is fed by a SMA connector with characteristic impedance of 50 ohm that is connected to the antenna using silver paste instead of solder to avoid damaging the printed surface with the hot soldering iron tip. The SMA connector is attached to the antenna through a coplanar-waveguide (CPW) section for impedance matching purposes.
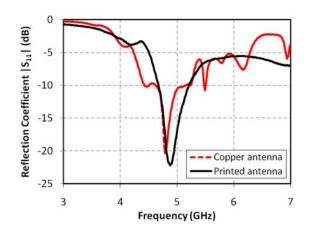

FIG. 4. The input reflection coefficient of the printed antenna compared to the reference antenna.

C. Printed antenna performance

In order to compare the performance of the printed antenna, a reference antenna made of copper was fabricated using the traditional printed-circuit-board (PCB) technology with a milling machine. The measured magnitude of the reflection coefficient $|S_{11}|$ at the input of the direct-write printed antenna is presented in Figure 4 and shows 22 dB return loss, which means that less than 1% of the power that is input to the antenna is reflected back to the transmitting source. This curve is also compared to the magnitude of the reflection coefficient of the reference copper antenna in the same figure. The measurement of the direct-write printed antenna $|S_{11}|$ shows a very good agreement with that of the reference antenna. Both antennas resonate at the 4.9 GHz frequency-band which is allocated to public safety applications.[26]

The radiation pattern of the antenna was measured in the anechoic chamber facility at the resonant frequency of 4.9 GHz and is depicted in Figure 5. As expected for this type of electromagnetic radiator that consists of an aperture without a back side ground plane or cavity backing, this antenna has an omnidirectional radiation pattern. This is typical and desired in good receivers and shows that the antenna receives energy from all directions in its main plane of radiation, perpendicular to the substrate. The direct-write printed antenna has also a very similar radiation pattern to the reference copper antenna, illustrating the suitability of
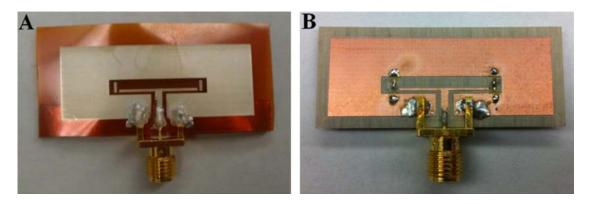

FIG. 3. (a) The direct-write printed CFSA and flexible folded-slot dipole antenna on Kapton® substrate. (b) Reference antenna made of copper.
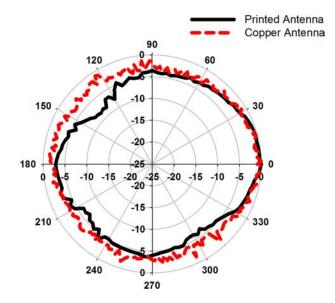
FIG. 5. Normalized radiation pattern of the printed CFSA and of the reference copper antenna in the principal radiation plane illustrating omnidirectionality and the suitability of the nanoinks for flexible antenna development.

the nanoinks to develop the entire structure without significantly affecting or degrading the antenna performance.

IV. CONCLUSIONS

In summary, the encapsulation of nanoparticles plays a key role in fabricating flexible electronics using metallic nanoparticulate inks. We have shown that the decomposition/desorption temperatures of the short-chain carboxylic acids from the silver nanoparticles depend on their chain length, and we utilized these particles to print a flexible antenna. This study also helps to select substrates suitable for printing and especially compatible with the sintering temperatures of the nanoparticles. The CFSA printed on Kapton® showed an excellent performance that matches well that of the copper reference antenna. These results will be useful to fabricate future flexible printed antennas using metallic nanoinks.

ACKNOWLEDGMENTS

[1]K. Ankireddy, S. Vunnam, J. Kellar, and W. Cross, J. Mater. Chem. C **1**, 572 (2013).
[2]B. Y. Ahn, E. B. Duoss, M. J. Motala, X. Guo, S. Park, Y. Xiong, J. Yoon, R. G. Nuzzo, J. A. Rogers, and J. A. Lewis, Science **323**, 1590 (2009).
[3]D. E. Anagnostou, A. A. Gheethan, A. K. Amert, and K. W. Whites, J. Disp. Technol. **6**, 558 (2010).
[4]S. H. Ko, J. Chung, H. Pan, C. P. Grigoropoulos, and D. Poulikakos, Sens. Actuators, A **134**, 161 (2007).
[5]V. Subramanian, J. M. J. Frechet, P. C. Chang, D. C. Huang, J. B. Lee, S. E. Molesa, A. R. Murphy, D. R. Redinger, and S. K. Volkman, Proc. IEEE **93**, 1330 (2005).
[6]A. M. Gaikwad, D. A. Steingart, T. N. Ng, D. E. Schwartz, and G. L. Whiting, Appl. Phys. Lett. **102**, 233302 (2013).
[7]I. Grunwald, E. Groth, I. Wirth, J. Schumacher, M. Maiwald, V. Zoellmer, and M. Busse, Biofabrication **2**, 014106 (2010).
[8]D. C. Kim and D. J. Kang, Sensors **8**, 6605 (2008).
[9]C. A. Bauer, F. Stellacci, and J. W. Perry, Top. Catal. **47**, 32 (2008).
[10]D. Huang, F. Liao, S. Molesa, D. Redinger, and V. Subramanian, J. Electrochem. Soc. **150**, G412 (2003).
[11]Y. Wu, Y. Li, P. Liu, S. Gardner, and B. S. Ong, Chem. Mater. **18**, 4627 (2006).
[12]M. J. Coutts, M. B. Cortie, M. J. Ford, and A. M. Mcdonagh, J. Phys. Chem. C **113**, 1325 (2009).
[13]T. Y. Dong, W. T. Chen, C. W. Wang, C. P. Chen, C. N. Chen, M. C. Lin, J. M. Song, I. G. Chen, and T. H. Kao, Phys. Chem. Chem. Phys. **11**, 6269 (2009).
[14]N. Nishida, M. Hara, H. Sasabe, and W. Knoll, Jpn. J. Appl. Phys., Part 1 **35**, 5866 (1996).
[15]N. Nishida, M. Hara, H. Sasabe, and W. Knoll, Jpn. J. Appl. Phys., Part 1 **36**, 2379 (1997).
[16]Z. Peng, H. You, and H. Yang, ACS Nano **4**, 1501(2010).
[17]A. Kamyshny, J. Steinke, and S. Magdassi, Open Appl. Phys. J. **4**, 19 (2011).
[18]M. L. Allen, K. Jaakkola, K. Nummila, and H. Seppa, IEEE Trans. Compon. Packag. Technol. **32**, 325 (2009).
[19]J. Siden, M. K. Fein, A. Koptyug, and H. E. Nilsson, IET Proc. Microwaves, Antennas Propag. **1**, 401 (2007).
[20]A. K. Sowpati, V. K. Palukuru, V. PynttÄari, R. MÄakinen, M. V. Kartikeyan, and H. Jantunen, Prog. Electromagn. Res. Lett. **13**, 59 (2010).
[21]Y. Kim, B. Lee, S. Yang, I. Byun, I. Jeong, and S. M. Cho, Curr. Appl. Phys. **12**, 473 (2012).
[22]K. J. Lee, Y. Lee, I. K. Shim, J. Joung, and Y. S. Oh, J. Colloid Interface Sci. **304**, 92 (2006).
[23]M. L. Connolly, Science **221**, 709 (1983).
[24]P. Gabbott, *Principles and Applications of Thermal Analysis* (Blackwell Publishing, Oxford, 2008), p. 5.
[25]S. Vunnam, K. Ankireddy, J. Kellar, and W. Cross, Thin Solid Films **531**, 294 (2013).
[26]A. Singer, *Application and Antenna Selection in the 4.9 GHz Band*, Microwave J. 2007, see http://www.microwavejournal.com/articles/5467-applications-and-antenna-selection-in-the-4-9-ghz-band?v=preview.